Supplemental Information

"Correlation of Vesicle Binding and Phospholipid Dynamics with Phospholipase C Activity: Insights into Phosphatidylcholine Activation and Surface Dilution Inhibition"

Pu,M., Fang, X., Redfield, A., Gershenson, A., and Roberts, M. F.

Dynamic light scattering measurements:

SUVs composed of different ratios of PC/PMe (X_{PC}) were analyzed by dynamic light scattering to extract r_{DLS}, the mass-weighted average radius of the vesicles. The data were obtained using a Protein Solutions DynaProdynamic light scattering instrument and analyzed with the Dynamics D5 software. Examples of distributions showing for pure PMe and pure PC vesicles are shown in Figure S1. The anionic-rich SUVs were slightly smaller with a narrower size distribution than PC-rich SUVs. The average radius for each vesicle preparation was calculated according to $R_{av.}=\Sigma_i \rho_i(r) R_i$, where $\rho_i(r)$ is the weight percentage of the corresponding radius (calculated from the Stokes-Einstein relation, $r=k_BT/6\pi\eta D$, where D is the diffusion coefficient measured by light scattering, k_B is Boltzmann's constant, T is the absolute temperature and η is the viscosity of the medium).

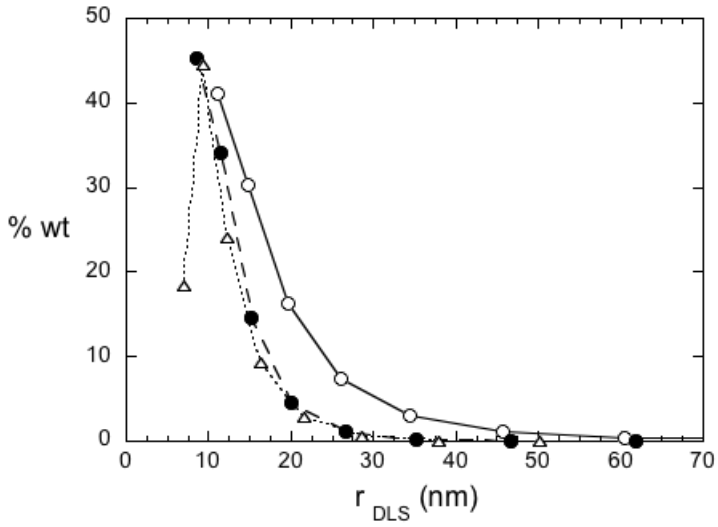

FIGURE S1. The mass-weighted size distribution (%wt) of single component PC (❍), PMe (●), and PG (Δ) SUVs (prepared by sonication) measured by dynamic light scattering. The radii were determined from the DLS data using the Stokes-Einstein relation.

The confocal FCS apparatus:

This setup is similar to that previously described for single pair Förster resonance energy transfer experiments (Liu et al., 2006). Briefly, the 488 nm line of an air-cooled argon-krypton laser (Melles-Griot) was used to excite the sample, a 500drlp dichroic mirror (Chroma Technology) reflected the laser light into a water objective (Olympus, NA=1.2) mounted on an inverted microscope (IX-70, Olympus). The same dichroic passed the fluorescence emission, and any remaining scattered laser light was blocked by a 505lp filter (Chroma Technology). A 30 μm confocal pinhole (Thor Labs) in the conjugate image plane was used to define the observation volume and to block out of focus fluorescence. The fluorescence

was collimated, split by a non-polarizing 50-50 beam splitter (Newport) and focused unto two avalanche photodiodes (APDs, SPCM-AQR-14, Perkin-Elmer). For AF488 labeled protein, HQ535/50 bandpass filters (Chroma Technology) before the focusing lenses blocked the Raman scattering. For rhodamine-labeled SUVs, the 520 nm laser line was used with a 535drlp dichroic mirror and HQ450lp longpass filter in the microscope, and the filters in front of the APDs were replaced by HQ645/75 bandpass filters (Chroma Technology). The photon counts from the APDs were collected by a 2-channel data acquisition card, and associated software was used to calculate and analyze the auto- and cross-correlations (ISS).

FCS – estimation of the diffusion constant D:

The auto and crosscorrelation, $G_{j,k}(\tau)$, are calculated from the time dependent fluorescence intensities. I(t), according to (Elson & Magde, 1974; Thompson, 1991):

$$G_{j,k}(\tau) = \frac{\langle \delta I_k(t) \delta I_k(t) \rangle}{\langle I_j(t) \rangle \langle I_k(t) \rangle} \qquad (1)$$

where $I_j(t)$ and $I_k(t)$ are the time dependent fluorescence signals detected in channels j and k respectively, < > indicates a time average, and j=k for the autocorrelations. $\delta I_k(t)$ is the time dependent fluorescence fluctuation on channel k and is given by $\delta I_k(t) = I_k(t) - \langle I_k(t) \rangle$. For one-photon excitation and a small, 30 μm, confocal pinhole, the observation volume can be approximated as a 3-dimensional Gaussian with radial and axial dimensions of ω_o and z_o respectively (Magde et al., 1974; Hess & Webb, 2002). If the solution contains only a single species diffusing in three dimensions, the correlation curves can be fit according to (Magde et al., 1974; Thompson 1991):

$$G(\tau) = \frac{1}{\langle N \rangle} \left(\left(1 + \frac{4D\tau}{\omega_o^2} \right) \sqrt{1 + \frac{4D\tau}{S^2 \omega_o^2}} \right)^{-1} \qquad (2)$$

where <N> is the time averaged number of molecules in the effective volume, D is the diffusion coefficient in μm^2/sec, and S is the ratio of the axial to the radial dimension ($S = z_o/\omega_o$). The diffusion time, τ_D, is given by $\tau_D = \omega_o^2/4D$. The observation volume defined by S and ω_o was characterized at the beginning and end of each day of experiments using the calibration dye rhodamine 110 or rodamine 6G with a reported diffusion coefficient of 280 μm^2/sec for rhodamine at 22°C (Magde et al., 1974). For 488 nm excitation, values of S were between 6.8 and 8 and values of ω_o ranged from 0.194 to 0.201 μm. The values of S and ω_o determined from global fits of the dye data were used to fit the protein and/or SUV data.

Analysis of high resolution ^{31}P field cycling:

The analysis of the magnetic field dependence of R_1 described in 'Experimental Procedures' (breaking the relaxation into two distinct field regimes) is based on a more complete treatment of the relaxation behavior covering the entire field range (a detailed discussion, particularly on using Woessner theory and a Liparo-Szabo formalism can be found at www.pnas.org/cgi/content/full/0407565101/DC1). What follows presents the theory for the different relaxation terms and discusses key assumptions that allow us to use the simplified analysis to obtain key parameters describing phospholipid headgroup dynamics.

The field dependence of R_1 can be described with the following general expression:

$$R_1 = R_{dv} + R_{dc} + C_L \omega_P^2 J(\tau_c, \omega_P) + C_H \omega_P^2 J(\tau_h, \omega_P), \qquad (3)$$

where the function $J(\tau, \omega)$ is $2\tau/(1+ (\omega\tau)^2)$ and

$$R_{dv} = R_v(0)\, D(\omega_H; \omega_P, \tau_v); \quad (4a)$$

$$R_{dc} = R_d(0)\, D(\omega_H; \omega_P, \tau_c). \quad (4b)$$

The first terms R_{dv} and R_{dc} are from the phosphorus-proton nuclear dipolar interaction, predominantly with the nearest protons on the glycerol and polar side chain, with assumed correlation times τ_v and τ_c, on the order of 10^{-6} and 10^{-8} s, respectively. The longer correlation time, τ_v, is due to overall rotational diffusion of the vesicle possibly combined with individual translational diffusion of a phospholipid about the vesicle surface (Roberts & Redfield, 2004b), while τ_c arises from internal motion within the phospholipid previously identified with diffusion-within a cone ("wobble") (Klauda et al., 2008). The function $D(\omega_H; \omega_P, \tau)$ is

$$D(\omega_H; \omega_P, \tau) = (2\tau)^{-1}\{[0.1\, J(\tau, \omega_H - \omega_P)] + [\{0.3\, J(\tau, \omega_P)]+[0.6\, J(\tau, \omega_H + \omega_P, \tau)]\}, \quad (4c)$$

and the parameters $R_v(0)$ and $R_d(0)$ are

$$R_v(0) = S_v^2\, \tau_v\, K_n\, r_{PH}^{-6}; \quad (4d)$$

$$R_c(0) = S_c^2\, \tau_c\, K_n\, r_{PH}^{-6}, \quad (4e)$$

where the order parameters S_v^2 and S_c^2 are the fractions for the noise power of the stochastically varying dipolar interactions with correlations times τ_v and τ_c respectively. K_n is a product of known constants (Roberts & Redfield, 2004a) including the squares of the gyromagnetic ratios of the nuclear spins involved (here phosphorus and protons). The expression "r_{PH}^{-6}" above is shorthand for $\Sigma\langle r_{PH}^{-3})^2\rangle$, where r_{PH} is the distance from the phosphorus to a particular proton, the $\langle\ \rangle$ denotes a time average, and Σ denotes a sum over all protons (in practice only the nearest ones).

The last two terms in Eq. 3 are the contribution of phosphorus chemical shift anisotropy (CSA). The factors C_L and C_H are

$$C_L = K_C\, S_C^2; \quad (5a)$$

$$C_H = 2\, \tau_h\, K_C\, (1-S_C^2), \quad (5b)$$

where K_C is a product of known constants including effectively the square of the size of the CSA interaction, and S_C^2 is the fraction of the CSA power spectrum with the same internal correlation time τ_c mentioned earlier. The last term in Eq. 3 results from fast short range fluctuations with times scale $\tau_h \sim 10^{-11}$ s.

Our fitting procedure is simplified as follows, in ways that do not affect the important output parameters. (i) We use the same correlation time τ_c and order parameter S_C^2 in the second and third terms of Eq. 3 even though these terms arise from different vectors in the phospholipid. The τ_c for the dipolar and CSA terms may differ, according to a simulation of pure dipalmitoylphosphatidylcholine vesicles, by a factor of 2-3 (Klauda et al., 2008). (ii) Eq. 3 omits the dipolar fluctuations with the high-frequency correlation time τ_h, and the CSA fluctuations with correlation time τ_v, neither of which are possible to observe with our method. However, all the order parameters for each interaction (dipolar, and CSA) must add to one so that $S_v^2 + S_c^2$ will be less than one, though probably not small compared to one; and the factor $(1-S_C^2)$ in Eq. 5b should be replaced by a smaller number. (iii) The spectral density $J(\tau_h, \omega_P)$ in the last term of Eq. 3 is replaced by $2\,\tau_h$, because $(\omega_P\tau_h)^2$ in its denominator is small compared to one.

While our fitting procedure may appear complex, in fact, much of what we use can be evaluated by eye directly from our data, without use of a computer. These will be illustrated with the field dependence for pure PMe SUVs (Figure S2). (i) The parameters $R_v(0)$ and $R_c(0)$ are the maximum low frequency

values of the two first (dipolar) terms of Eq. 3, and are easily estimated because the other (CSA) terms are negligible at the low fields (below ~2 T) where these dispersions are large. They can be evaluated directly because the correlation times involved are so different (~1 μs versus ~10 ns). $R_c(0)$ is close to the value of R_1 at around 0.1 T for our samples, and the sum of $R_v(0)$ and $R_c(0)$ is estimated by the limit of R_1 at zero field (in practice at ~0.003 T). The correlation time τ_v is likewise fairly well estimated from the field at which R_1 is midway between $R_v(0)$ and $R_c(0)$, divided by the proton gyromagnetic ratio, because the function D (Eq. 4c) is approximately equal to 1/2 when $\omega_H \tau = 1$ (Figure S2A). The internal correlation time τ_c can likewise be estimated (less accurately because of the contribution from CSA) from the half point in field between where $R_1 \sim R_c(0)$ and where it becomes nearly independent of field, around 2 T. We can use changes in $R_c(0)$ to estimate changes in τ_c according to Eq. 4d if S_c^2 and r_{PH}^{-6} are nearly constant. For comparison, the R_1 field dependence above 0.07 T is broken down into dipolar and CSA terms with τ_c, as well as the CSA term for the faster motion characterized by τ_h (Figure S2B).

Finally, the parameter S_C^2, as deduced from the field variation of CSA relaxation above about 5 T, has been found to be a useful indicator of internal dynamics for nucleic acids (Roberts et al., 2004). It can be determined from the ratios of the last 2 terms of Eq. 3 because the dipolar terms are negligible at high fields. The correlation time τ_h cannot be determined as easily, but it can be estimated from the size of the square-law variation of Eq. 5b, by iterative fitting of the high-field rates.

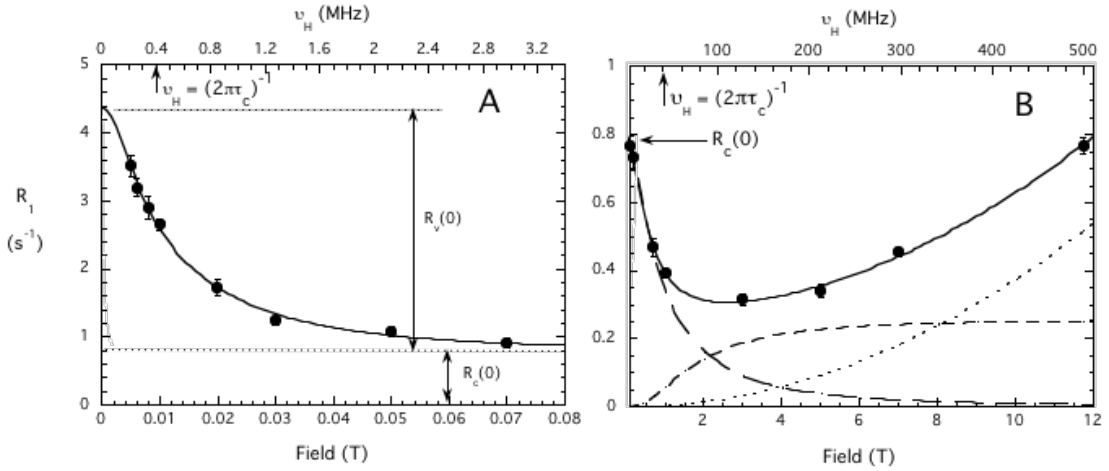

FIGURE S2. Field dependence of the ^{31}P R_1 for PMe in pure PMe SUVs at 25°C. For clarity, two magnetic field ranges are shown in the two panels with different field and relaxation rate scales: (A) low field region from 0 to 0.08 T; (B) region from 0.1 to 12 T. The upper x-axis shows the ^1H frequency scale for comparison. The lines represent best fits of (A) total dipolar $R_1 = R_{dv} + R_{dc}$, and (B) $R_{dc} + C_L \omega_P^2 J(\tau_c, \omega_P) + C_H \omega_P^2 J(\tau_h, \omega_P)$. Arrows indicate R(0) in each region as R_1 is extrapolated to zero field. Arrows on the upper ^1H frequency scale indicate how τ_v and τ_c can be visually estimated from the approximate half-point of the R_1 dispersion. In (B), the fitted relaxation contributions from the last three terms of Eq. 3 are shown, as a long-dashed curve for the second (dipolar) term, and a short dashed curve, and a dotted curve, for the two last (CSA) terms respectively.

References:

Elson, E. L., and Magde, D. (1974) Fluorescence correlation spectroscopy I. Conceptual basis and theory, *Biopolymers* **13**, 1-27.

Hess, S. L., and Webb (2002) Focal volume optics and experimental artifacts in confocal fluorescence correlation spectroscopy, *Biophys. J.* **83**, 2300-2317.

Klauda, J. B., Roberts, M. F., Redfield, A. G., Brooks, B. R., and Pastor, R. W. (2008) Rotation of lipids in membranes: MD simulation, ^{31}P spin-lattice relaxation, and rigid-body dynamics, *Biophys J.* **94**, 3074-3083.

Liu, L., Mushero, N., Hedstrom, L., and Gershenson, A. (2006) Conformational distributions of protease-serpin complexes: a partially translocated complex, *Biochemistry* **45**, 10865-10872.

Magde, D., Elson, E. L. and Webb, W. W. (1974) Fluorescence correlation spectroscopy. II. An experimental realization, *Biopolymers* **13**, 29–61.

Roberts, M. F., and Redfield, A. G. (2004a) High-resolution ^{31}P field cycling NMR as a probe of phospholipid dynamics, *J. Am. Chem. Soc.* **126**, 13765-13777.

Roberts, M. F., and Redfield, A. G. (2004b) Phospholipid bilayer surface configuration probed quantitatively by ^{31}P field-cycling NMR, *Proc. Natl. Acad. Sci. U. S. A.* **101**, 17066-17071.

Roberts, M. F., Cui, Q., Turner, C. J., Case, D. A., and Redfield, A. G. (2004) High-resolution field-cycling NMR studies of a DNA octamer as a probe of phosphodiester dynamics and comparison with computer simulation, *Biochemistry* **43**, 3637-3650.

Thompson, N. L. (1991) Fluorescence correlation spectroscopy, in *Topics in Fluorescence Microscopy* (J. Lakowicz, editor), Plenum Press, New York, pp. 337–378.